Multiaffinity and entropy spectrum of self-affine fractal profiles

Hiroaki Katsuragi* and Haruo Honjo†
Department of Applied Physics, Faculty of Engineering, Kyushu University, Ropponmatsu, Fukuoka 810-8560, Japan
(Received 10 December 1997)

The entropy spectrum method is applied to self-affine fractal profiles. First, the profile created by a generalized multiaffine generator is decomposed into many subsets having their own topological entropies. The entropy spectrum and H_q (the qth Hurst exponent) of its profile is calculated exactly. For each subset, D_D (divider dimension) and D_B (box dimension) are also calculated. The relation $D_B=2-H_{q=1}$ is obtained for the remaining subset after infinite iteration of the generator. Next, the entropy spectrum of fractional Brownian motion (FBM) traces is examined and obtained as a point spectrum. This implies that a variety of lengths of segments in FBM traces is caused not by intrinsic inhomogeneity or mixing of the Hurst exponents but by only the trivial fluctuation. Namely, there are no fluctuations in singularity or in topological entropy. Finally, a real mountain range (the Hida mountains in Japan) is also analyzed by this method. Despite the profile of the Hida mountains having two Hurst exponents, the entropy spectrum of its profile becomes a point spectrum again. [S1063-651X(99)10901-2]

PACS number(s): 47.53.+n, 05.40.−a, 92.40.Gc

I. INTRODUCTION

In nature, there are many complex patterns such as coastlines, clouds, and cracks. Though it seems that quantitative analysis of these complex patterns is impossible at a glance, the fractal concept enables us to analyze them quantitatively [1]. The scaling exponent between the utilized unit size and the number of units to cover the object is very useful to quantify these complex patterns and is called the fractal dimension. The concept of the fractal has become very famous now and has been expanded.

Many patterns are scaled differently in different directions, for example, fracture surfaces of metals [2], crystallization of NH_4Cl [3], wet front propagation in paper [4], real mountain topography [5,6] and so on [7,8]. These anisotropic patterns are called self-affine fractals and are characterized by the Hurst exponent (or roughness exponent) H $(0<H<1)$ [7]. We consider a single-valued function of a single variable $F(t)$. If the function is a self-affine fractal, the function satisfies the scaling relation

$$F(t)\simeq\xi^{-H}F(\xi t), \tag{1}$$

where ξ is a parameter. In stochastic systems, the height-height correlation function $C(t)$ can be evaluated. For a statistical self-affine function, $C(t)$ is written as

$$C(t)=\langle|F(t')-F(t'+t)|\rangle_{t'}\propto t^H, \tag{2}$$

where angular brackets denote an average quantity. In the single-valued self-affine function, the fractal dimension shows different values depending on measuring methods. It is well known that the *local* divider dimension D_D and the *local* box dimension D_B are related to H as [9,10]

$$D_D=\frac{1}{H}, \tag{3a}$$

$$D_B=2-H. \tag{3b}$$

These relations hold only on profiles whose topological dimension is unity that are embedded in two-dimensional Euclidean space. In addition, Eq. (3a) holds for $H\geqslant\frac{1}{2}$. For $H<\frac{1}{2}$, $D_D=2$ [10]. Moreover, both D_D and D_B become unity on a *global* scale [11]. However, these relations (3a) and (3b) are very useful for investigation of self-affine fractals due to the easier measurements of D_D and D_B and the dominance of $H\geqslant\frac{1}{2}$ in nature.

On the other hand, limitations of only one fractal dimension for self-similar fractals have been realized. Thus fractal measures characterized by an infinite hierarchy of fractal dimensions have been researched [12,13]. This multifractal insight provides much detailed understanding [11]. The multifractal property has been usually studied by the $f(\alpha)$ spectrum obtained from a thermodynamic formalism. In the formalism a partition function is defined and the $f(\alpha)$ spectrum is obtained from the Legendre transform. This $f(\alpha)$ spectrum method can describe the static fluctuations of singularity of the probability measure and fractal dimension.

Recently, Barabási *et al.* have reported multifractality of self-affine fractals [14,15]. They have investigated a multiaffine function created by a simple generator and have obtained a multifractal spectrum. They have calculated the qth-order height-height correlation function $C_q(t)$ as

$$C_q(t)=\langle|F(t')-F(t'+t)|^q\rangle_{t'} \tag{4}$$

*Present address: New Science Department, Mitsubishi Research Institute, Inc., 3-6 Ohtemachi 2-Chome, Chiyoda-ku, Tokyo 100-8141, Japan.

†Present address: Department of Applied Science for Electronics and Materials, Interdisciplinary Graduate School of Engineering Sciences, Kyushu University, Kasuga 816-8580, Japan.

and defined the generalized Hurst exponent H_q in the limit $t \to 0$ of

$$C_q(t) \propto t^{qH_q}. \tag{5}$$

If H_q varies with q, a nontrivial multiaffine spectrum is obtained. This analysis corresponds to the multifractal method and its thermodynamic formalism is defined in Ref. [15].

In contrast to the $f(\alpha)$ spectrum, the entropy spectrum has been studied in order to describe the dynamical property. This entropic analysis has also been defined by the thermodynamic formalism and has been applied to chaotic dynamics [16,17]. Sano *et al.* have investigated fluctuations of Lyapunov exponents and topological entropy such as the relationships among dimensions of invariant measures, Lyapunov exponents and entropies, the strange attractor vs repeller, and the variational principle [16]. In general, the entropy function of hyperbolic dynamical systems has been obtained by Bohr and Rand [18]. Honjo and Sano have studied self-similar fractal patterns by the entropy spectrum method [19]. They have obtained entropy spectra of self-similar fractal patterns with multiscaling factors. Each pattern has been decomposed into many fractal subsets of different similarity dimensions whose maximum value corresponds to the similarity dimension of the whole pattern. They have discussed the dynamical behavior of the subsets using the entropy spectrum. The multifractal spectrum and entropy spectrum are very similar but not identical. The main difference between the two spectra is the definition of the singularity of subsets, which is defined to the support size in the former and the time step in the latter to describe the dynamics of pattern formation [19]. Hence the entropy spectrum method can describe fluctuations of topological entropy and singularity to the time step. Namely, we can examine how microstructures appear associated with the time step by the entropy spectrum method.

To the best of our knowledge, there is no report on the entropy spectrum of self-affine fractal profiles. In this paper we apply the entropy spectrum method to self-affine fractal profiles. One of our purposes, is to understand the appearing behavior of microstructures in self-affine fractal profiles. For example, a random time series is only the folded line in the early stage and its profile becomes complicated by long time observation. This complicated process resembles the iterative process of the generator. Therefore, we investigate the detailed evolution of generalized multiaffine generators. A parameter that is independent of the time step is introduced instead of using the thermodynamic formalism. It is useful for the investigation of profiles created by contraction maps because the topological entropy, singularity, divider dimension, and box dimension are calculable for each subset. In succession, this method is applied to fractional Brownian motion (FBM) traces [20] as a random time series. Real mountain profiles (the Hida mountains in Japan) are also analyzed as an example of the real self-affine fractal profiles in nature. Finally, the comparison between the entropy spectrum and multiaffine spectrum is discussed.

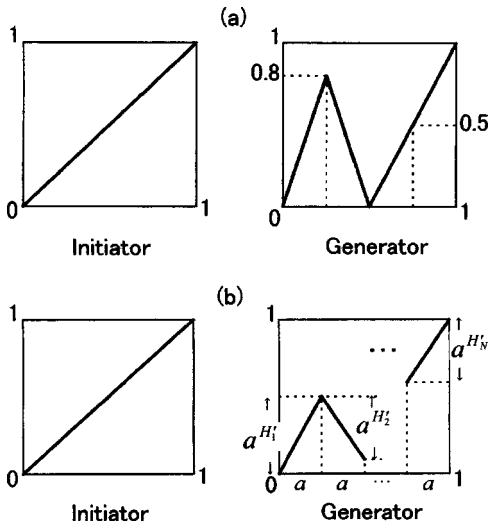

FIG. 1. (a) The initiator is a diagonal line of a square. The generator has four contraction maps and two different scaling factors $\frac{4}{5}$ $(=a^{H'_1}=a^{H'_2})$ and $\frac{1}{2}$ $(=a^{H'_3}=a^{H'_4})$ in the vertical direction. All of the segments have the same horizontal contraction ratio $a = \frac{1}{4}$. (b) The initiator is a diagonal line of a square. The generator consists of N contraction maps. The ith segment has the same horizontal contraction ratio a and different vertical contraction ratio $a^{H'_i}$.

II. ENTROPY SPECTRUM AND DIMENSIONS OF GENERALIZED MULTIAFFINE PROFILES

A. Formulation

Barabási *et al.* have worked with a simple multiaffine generator [Fig. 1(a)] [14]. The initiator is a diagonal line of a square whose side is unity. The generator has the same horizontal contraction ratio $\frac{1}{4}$ and two different vertical contraction ratios $\frac{4}{5}$ and $\frac{1}{2}$. Mixing of these different contraction ratios results in the multiaffinity described by variable H_q. This generator is a simple example. Thus we consider the generalized multiaffine generator [Fig. 1(b)] and discuss H_q and the entropy spectrum.

The generator consists of N segments, which have the same horizontal contraction ratio a $(=1/N)$ and different vertical contraction ratios $a^{H'_i}$ in the ith segment $(i = 1,2,\ldots,N)$. Here H'_i describes the anisotropy of scaling in each segment. If $H'_i = H$ (const) for all i, the profile at an infinite iteration time $(n=\infty)$ certainly has one (not multiple) Hurst exponent H. If each H'_i is different, various vertical lengths are yielded by the combination of different contraction ratios. Therefore, we are interested in vertical lengths of individual segments. We focus on whether or not the singularity of the probability measure being proportional to the vertical lengths of individual segments fluctuates. Furthermore, the vertical lengths of the segments are very important for calculations of the height-height correlation function, divider dimension, and box dimension.

We consider a segment whose vertical length is $l_n(\boldsymbol{k}) = a^{(H'_1 k_1 + H'_2 k_2 + \cdots + H'_N k_N)}$ at the nth step. Here the vector $\boldsymbol{k}$ is $\boldsymbol{k}=(k_1,k_2,\ldots,k_N)$, k_i is an integer $(0 \leqslant k_i \leqslant n)$, and $\Sigma_{i=1}^{N} k_i = n$. The total vertical length of segments is written as $L_n = (a^{H'_1} + a^{H'_2} + \cdots + a^{H'_N})^n$. The probability measure of the segment is $p_n(\boldsymbol{k}) = l_n(\boldsymbol{k})/L_n$. From the above definitions,

$l_n(\boldsymbol{k})$, the number of segments $N_n(\boldsymbol{k})$, and $p_n(\boldsymbol{k})$ are obtained as

$$l_n(\boldsymbol{k})=\prod_{i=1}^{N} a^{H_i' k_i}, \tag{6a}$$

$$N_n(\boldsymbol{k})={}_nC_{k_1}\,{}_{n-k_1}C_{k_2}\cdots{}_{n-k_1-\cdots-k_{N-1}}C_{k_N}, \tag{6b}$$

$$p_n(\boldsymbol{k})=\frac{\prod_{i=1}^{N} a^{H_i' k_i}}{\left(\sum_{i=1}^{N} a^{H_i'}\right)^n}. \tag{6c}$$

We assume that for $n\gg 1$, $l_n(\boldsymbol{k})$, $N_n(\boldsymbol{k})$ and $p_n(\boldsymbol{k})$ could depend on n as

$$l_n(\boldsymbol{x})=\exp[-n\delta(\boldsymbol{x})], \tag{7a}$$

$$N_n(\boldsymbol{x})=\exp[nh(\boldsymbol{x})], \tag{7b}$$

$$p_n(\boldsymbol{x})=\exp[-n\lambda(\boldsymbol{x})]. \tag{7c}$$

Here the vector $\boldsymbol{x}$ is $\boldsymbol{x}=(x_1,x_2,\ldots,x_N)$ and $x_1=k_1/n, x_2=k_2/n,\ldots,x_N=k_N/n$ ($\Sigma_{i=1}^{N}x_i=1$, $0\leqslant x_i\leqslant 1$). $\delta(\boldsymbol{x})$ is the decay exponent of the vertical length of the segment, $h(\boldsymbol{x})$ is the increasing exponent of the number and represents the topological entropy of the segment, and $\lambda(\boldsymbol{x})$ is the decay exponent of the probability measure of the segment. From $h(\boldsymbol{x})$ and $\lambda(\boldsymbol{x})$, the $h(\lambda)$ spectrum is obtained, i.e., $h(\boldsymbol{x})$ and $\lambda(\boldsymbol{x})$ are parameter descriptions of $h(\lambda)$. Then we divide the prefractal [11] profile set S_n at the nth step into subsets $S_n(\lambda(\boldsymbol{x}))$ characterized by $\lambda(\boldsymbol{x})$,

$$S_n=\bigcup_{\lambda(\boldsymbol{x})} S_n(\lambda(\boldsymbol{x})). \tag{8}$$

For $n\gg 1$, explicit forms of $\delta(\boldsymbol{x})$, $h(\boldsymbol{x})$, and $\lambda(\boldsymbol{x})$ are calculable as

$$\delta(\boldsymbol{x})=-\sum_{i=1}^{N} H_i' x_i \ln a, \tag{9a}$$

$$h(\boldsymbol{x})=-\sum_{i=1}^{N} x_i \ln x_i, \tag{9b}$$

$$\lambda(\boldsymbol{x})=\ln\left(\sum_{i=1}^{N} a^{H_i'}\right)-\sum_{i=1}^{N} H_i' x_i \ln a. \tag{9c}$$

Note that $\delta(\boldsymbol{x})$, $h(\boldsymbol{x})$, and $\lambda(\boldsymbol{x})$ are independent of n. There are some characteristic subsets. The maximum value of the $h(\lambda)$ spectrum $h_{\max}(=\ln N)$ corresponds to the increasing ratio of all segments at each iteration. From Eqs. (9b) and (9c), we can find that the subset satisfying $x_i=a$ $(i=1,2,\ldots,N)$ has this maximum value ($h_{\max}$). Namely, in the $h(\lambda)$ spectrum, there is a unique maximum value corresponding to the topological entropy of the entire pattern. The probability of the subset $S_n(\lambda(\boldsymbol{x}))$ can be written as $P_n(\lambda(\boldsymbol{x}))=N_n(\lambda(\boldsymbol{x}))p_n(\lambda(\boldsymbol{x}))=\exp[-n\{\lambda(\boldsymbol{x})-h(\lambda(\boldsymbol{x}))\}]$ and $\lambda(\boldsymbol{x})-h(\lambda(\boldsymbol{x}))\geqslant 0$. Thus only the subset whose $h(\lambda(\boldsymbol{x}))$ is equal to $\lambda(\boldsymbol{x})$ remains at $n=\infty$; $h(\boldsymbol{x})=\lambda(\boldsymbol{x})\equiv\lambda^*$ and $P_{n=\infty}(\lambda^*)=1$. Moreover, the corresponding entropy h^* $(=\lambda^*)$ denotes the information entropy [11] of the generator; $h^*=-\Sigma_{i=1}^{N} r_i \ln r_i$. Here $r_i=a^{H_i'}/\Sigma_{i=1}^{N} a^{H_i'}$ is the probability of the segment (the vertical length normalized to the total vertical length of the generator). $\delta(\boldsymbol{x})$ is related to $\lambda(\boldsymbol{x})$ as $\delta(\boldsymbol{x})=\ln(L_1)+\lambda(\boldsymbol{x})$.

H_q of this profile is also calculable. The exact form of the qth-order height-height correlation function is written as

$$\begin{aligned} C_q(a^n)&=\sum_{k_1+\cdots+k_N=n} a^n\,{}_nC_{k_1}\cdots \\ &\quad\times{}_{n-k_1-\cdots-k_{N-1}}C_{k_N}\,a^{qH_1'k_1+\cdots+qH_N'k_N} \\ &=[a(a^{qH_1'}+\cdots+a^{qH_N'})]^n=(a^n)^{qH_q}. \end{aligned}$$

Thus

$$H_q=\frac{\ln\left(\sum_{i=1}^{N} a^{1+qH_i'}\right)}{q\ln a}. \tag{9d}$$

Here we improve the expression of H_q in Refs. [8,14,15,21]. In those papers H_q was obtained as $H_q=\ln[(b_1{}^q+b_2{}^q)/2]/q\ln(1/4)$. According to Eq. (9d), however, H_q of their model should be written as $H_q=\ln[\{2b_1{}^q+b_2{}^q+(1-b_2)^q\}/4]/q\ln(1/4)$ in general. The expression in those papers holds only for $b_2=0.5$.

The relations among the divider dimension D_D, box dimension D_B, and generalized Hurst exponent H_q are interesting problems. In order to examine these relations, we calculate D_D and D_B of the subset $S_n(\lambda(\boldsymbol{x}))$. $D_D(\boldsymbol{x})$ is obviously written as follows

$$D_D(\boldsymbol{x})=-\frac{\ln\{N_n(\boldsymbol{x})\}}{\ln\{l_n(\boldsymbol{x})\}}=\frac{h(\boldsymbol{x})}{\delta(\boldsymbol{x})}=\frac{\sum_{i=1}^{N} x_i\ln x_i}{\sum_{i=1}^{N} H_i' x_i \ln a}. \tag{9e}$$

Next we calculate $D_B(\boldsymbol{x})$. We consider the box number $M_n(\boldsymbol{x})$ required to cover the vertical length $l_n(\boldsymbol{x})$ by squares whose length of each side is ϵ_n. ϵ_n is written as $\epsilon_n=a^n$. Then $M_n(\boldsymbol{x})$ is obtained as

$$M_n(\boldsymbol{x})=\frac{\prod_{i=1}^{N} a^{H_i' x_i n}}{a^n}=\prod_{i=1}^{N}(a^{H_i'-1})^{nx_i}.$$

Thus the box dimension $D_B(\boldsymbol{x})$ is derived as

$$D_B(\boldsymbol{x})=-\frac{\ln\{N_n(\boldsymbol{x})\cdot M_n(\boldsymbol{x})\}}{\ln\{\epsilon_n\}}=1-\sum_{i=1}^{N} H_i' x_i+\frac{\sum_{i=1}^{N} x_i\ln x_i}{\ln a}. \tag{9f}$$

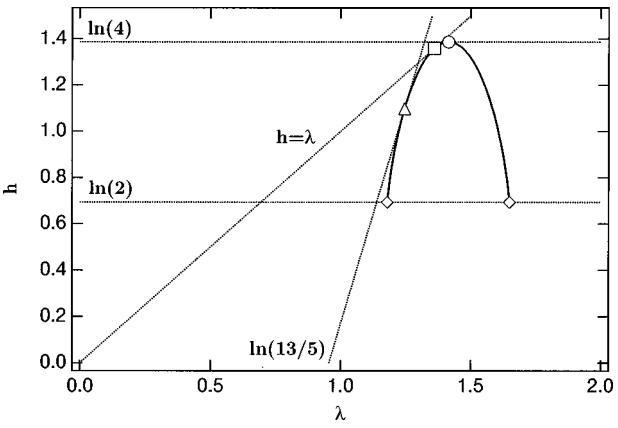

FIG. 2. Entropy spectrum of the profile created by the generator of Fig. 1(a). The topological entropy of the entire profile corresponds to the maximum value of the spectrum, ln4 (open circle). The topological entropy of the longest and the shortest segments are ln 2 (open diamonds). The remaining subset at $n=\infty$ is characterized by $x=\frac{8}{13}$ (open square). The subset shown by the open triangle gives the maximum value of $D_D(x)$.

The relations $D_D=1/H'(\boldsymbol{x})$ and $D_B=2-H'(\boldsymbol{x})$ hold for the subset whose topological entropy is maximum ($x_i=a$), where $H'(\boldsymbol{x})$ denotes the anisotropy of scaling of the subset $[H'(\boldsymbol{x})=\Sigma_{i=1}^{N}H_i'x_i]$. $D_D(\boldsymbol{x})$ is the same as the similarity dimension D_S of self-similar fractal patterns [19]. Therefore, the maximum value of D_D is obtained from the maximum value of the slope of the connecting line from ($\ln L_1$,0) to the $h(\lambda)$ spectrum in λ-h space. On the other hand, $2-H_1$ can be written as

$$2-H_1=2-\frac{\ln\left(\sum_{i=1}^{N}a^{H_i'+1}\right)}{\ln a}=1-\frac{\ln\left(\sum_{i=1}^{N}a^{H_i'}\right)}{\ln a}. \quad (10)$$

From Eqs. (9f) and (10) and $h(\boldsymbol{x})=\lambda(\boldsymbol{x})$, i.e., $-\Sigma_{i=1}^{N}x_i\ln x_i=\ln(\Sigma_{i=1}^{N}a^{H_i'})-\Sigma_{i=1}^{N}H_i'x_i\ln a$, the remaining subset at $n=\infty$ satisfies

$$2-H_1=1-\sum_{i=1}^{N}H_i'x_i+\frac{\sum_{i=1}^{N}x_i\ln x_i}{\ln a}=D_B(\boldsymbol{x}). \quad (11)$$

Equation (11) indicates that the relation (3b) holds only for $q=1$ in multiaffine profiles.

B. Simple example

A simple example studied by Barabási *et al.* is investigated here again from the viewpoint of the entropy spectrum [Fig. 1(a)] [14]. Because the generator has only two vertical contraction ratios $\frac{4}{5}$ (for i=1,2) and $\frac{1}{2}$ (for i-3,4), the vector (x_1,x_2,x_3,x_4) can be represented by one variable x $(=x_1+x_2;\ 1-x=x_3+x_4)$ and $0\leqslant x\leqslant 1$. Then $\delta(x)$, $h(x)$, and $\lambda(x)$ for $n\gg 1$ are obtained as

$$\delta(x)=\ln\frac{13}{5}-x\ln\frac{4}{5}-(1-x)\ln\frac{1}{2}=\ln\frac{13}{5}+\lambda(x), \quad (12a)$$

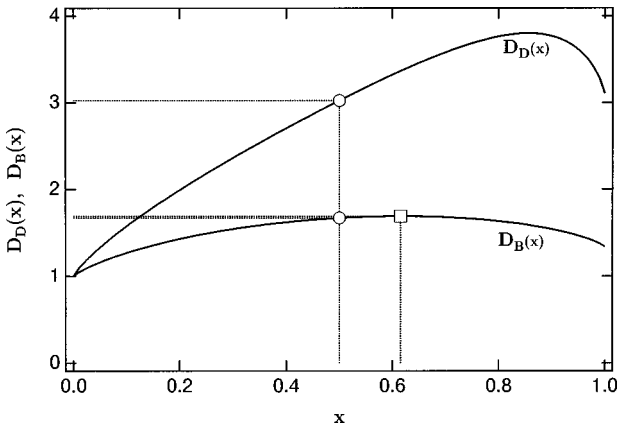

FIG. 3. $D_D(x)$ (divider dimension) and $D_B(x)$ (box dimension) of the subset $S_n(\lambda(x))$ of the profile created by the generator of Fig. 1(a). The subset whose h shows the maximum ($x=\frac{1}{2}$) satisfies $D_D(x)=1/H'(x)$ and $D_B(x)=2-H'(x)$ (open circles). The subset that remains at $n=\infty$ satisfies $D_B(x)=2-H_{q=1}$ (open square).

$$h(x)=\ln 2-x\ln x-(1-x)\ln(1-x), \quad (12b)$$

$$\lambda(x)=-x\ln\frac{4}{5}-(1-x)\ln\frac{1}{2}. \quad (12c)$$

We show the $h(\lambda)$ spectrum in Fig. 2. The maximum value of the spectrum is ln 4, which corresponds to the increasing ratio of segments of the entire pattern. The subset characterized by $x=\frac{1}{2}$ (open circle in Fig. 2) gives this maximum value of h and certainly increases by 4^n. The subsets of the longest segments $S_n(\lambda(1))$ and the shortest segments $S_n(\lambda(0))$ have the same minimum value of h, ln 2 (open diamonds in Fig. 2). This means that the number of these subsets increases by 2^n. The remaining subset at $n=\infty$ is characterized by $x=\frac{8}{13}$ (open square in Fig. 2).

H_q, D_D, and D_B are also calculable as

$$H_q=\frac{\frac{1}{4}\left[2\left(\frac{4}{5}\right)^q+2\left(\frac{1}{2}\right)^q\right]}{q\ln a}, \quad (12d)$$

$$D_D(x)=\frac{\ln 2-x\ln x-(1-x)\ln(1-x)}{-x\ln\frac{4}{5}-(1-x)\ln\frac{1}{2}}, \quad (12e)$$

$$D_B(x)=\frac{3}{2}+\frac{1}{\ln 4}\left[x\ln\frac{4}{5x}+(1-x)\ln\frac{1}{2(1-x)}\right]. \quad (12f)$$

Figure 3 shows $D_D(x)$ and $D_B(x)$. The relations $D_D(x)=1/H'(x)$ and $D_B(x)=2-H'(x)$ hold for the subset characterized by $x=\frac{1}{2}$ (open circles in Fig. 3). The remaining subset $S_n(\lambda(\frac{8}{13}))$ satisfies the relation (11) (open square in Fig. 3). Furthermore, the maximum value of $D_B(x)$ coincides with that of the remaining subset $D_B(\frac{8}{13})$. $D_D(x)$ is over 2 in almost all subsets; therefore, its value is meaningless even in the subsets characterized by $x=\frac{1}{2}$ or $x=\frac{8}{13}$. The maximum value of $D_D(x)$ numerically corresponds to the maximum value of $h/(\lambda-\ln L_1)$ as predicted in Sec. II A (open triangle in Fig. 2).

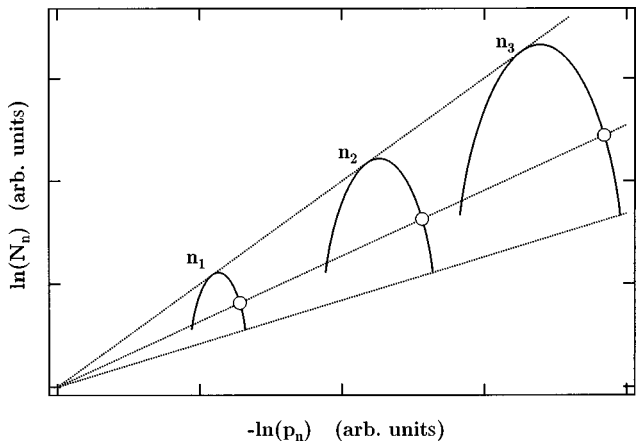

FIG. 4. Probability distribution curves ($\ln N_n$ versus $-\ln p_n$) of the prefractal profile created by the generator shown in Fig. 1(a) at arbitrary time steps n_1, n_2, n_3. The subset is composed of crossing points among these distribution curves and the line from the origin of coordinate axes. The open circles compose the subset characterized by $x=\frac{1}{10}$.

Written as above, the entropy spectrum and dimensions are calculable easily if the generator is given. However, it is too difficult to find the generator on the given pattern. Alternatively, there is another chance to obtain the entropy spectrum from the given pattern. From Eqs. (7a) and (7c) the relations $nh(\boldsymbol{x})=\ln N_n(\boldsymbol{x})$ and $n\lambda(\boldsymbol{x})=-\ln p_n(\boldsymbol{x})$ are obtained. Thus the log-log plots of the probability distribution curves of segments varying n give distribution curves *similar* to the entropy spectrum. Figure 4 shows these distribution curves of the prefractal profiles created by the generator of Fig. 1(a). The subset is composed of the crossing points among distribution curves and the line from the origin of the coordinate axes (open circles in Fig. 4 represent the subset characterized by $x=\frac{1}{10}$). Then $h(\boldsymbol{x})$ and $\lambda(\boldsymbol{x})$ are obtained in each subset from the n dependence of $\ln N_n$ and $-\ln p_n$, respectively. After that, the entropy spectrum can be obtained.

III. SPECIFIC APPLICATION

A. Fractional Brownian motion

Up to now we have discussed contraction maps in a formal way. This method should be applied to more specific self-affine profiles. We analyze FBM traces as a typical example of self-affine fractal profiles such as random time series. FBM traces are produced by a successive random addition method [22]. Vertical and horizontal axes are normalized to closed intervals $[0,1]$ at each step. We define the time step n as $n=\log_2 M$, where M is the total number of segments. This n is equivalent to the resolution level of the horizontal axis. The vertical length of each segment is normalized to its total sum and this normalized length is assigned to the probability measure p_n. We employ the cutoff scale of p_n as $\min\{p_n\}=2^{-n+11}\times 10^{-5}$. This cutoff scale is determined by the compromise between the computing time and the precision of the data. The probability measure p_n is replaced by $p_n=2^{-n+11}\times 10^{-5}(\kappa+\frac{1}{2})$ for the segment

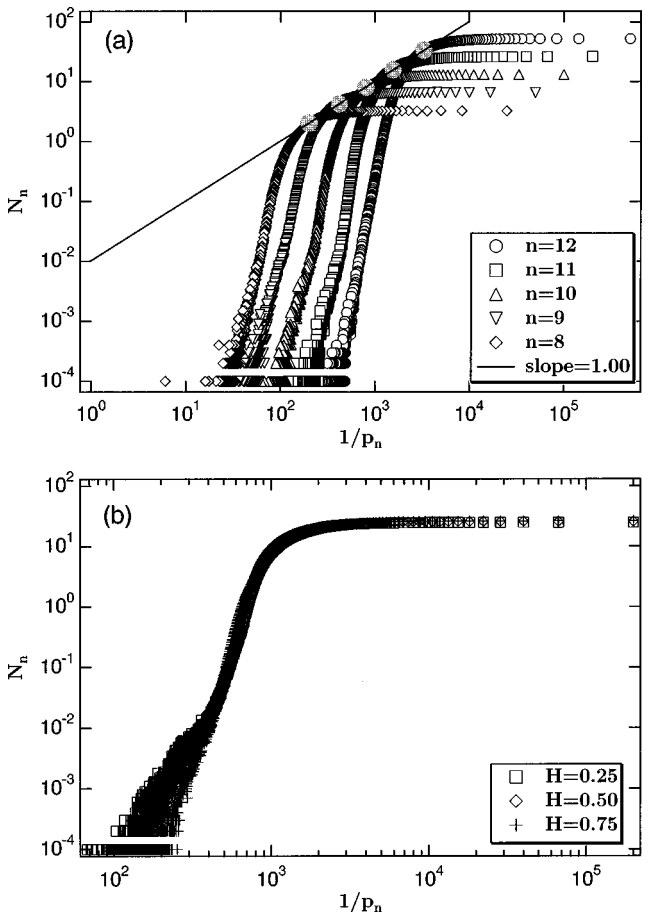

FIG. 5. (a) Double logarithmic plots of N_n versus $1/p_n$ on FBM traces ($H=0.75$). Gray circles indicate the subset whose probability $P_n=N_n p_n$ shows the maximum. (b) Double logarithmic plots of N_n versus $1/p_n$ on FBM traces that have different Hurst exponents ($H=$ 0.25, 0.50, and 0.75) at $n=11$.

whose p_n is $2^{-n+11}\times 10^{-5}\kappa \leqslant p_n < 2^{-n+11}\times 10^{-5}(\kappa+1)$, where κ is a non-negative integer. The number of segments is counted as $N_n(p_n)$.

In order to compose the subset, log-log plots of N_n versus $1/p_n$ at various n are shown in Fig. 5(a). Each distribution curve is obtained from an average of 10 000 FBM traces whose H is 0.75. The case of $H=0.75$ seems to be a particular case; however, these distribution curves are independent of H, as we will discuss later. In Fig. 5(b) the distribution curves of different H's at $n=11$ are shown and one can realize the coincidence of these distribution curves. The most interesting property of these distribution curves in Fig. 5(a) is the *congruence*. It should be recalled that the distribution curves in the case of contraction maps are *similar* to each other.

What makes this difference? The important difference between FBM traces and profiles created by the generator is the q dependence of H_q. The former has constant $H_q=H$ and the latter has a continuously changing nontrivial function H_q associated with q [14]. If H_q is constant, the vertical length of the segment l_n, the total vertical length L_n, and the number N_n are scaled by the time variation $n\rightarrow n-\log_2 b$ (this transformation is equivalent to $a\rightarrow ba$ for the horizontal length of each segment a and some parameter b) as

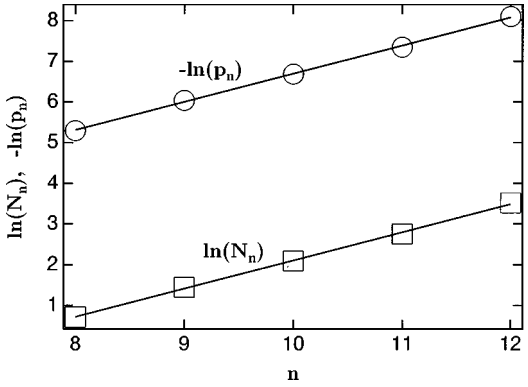

FIG. 6. n dependence of $\ln N_n$ and $-\ln p_n$ in the subset indicated by gray circles in Fig. 5(a). The slope of $\ln N_n$ and $-\ln p_n$ gives $h=0.691$ and $\lambda=0.691$, respectively.

$$l_n \rightarrow l_{n-\log_2 b} = b^H l_n , \tag{13a}$$

$$L_n \rightarrow L_{n-\log_2 b} = b^{H-1} L_n , \tag{13b}$$

$$N_n \rightarrow N_{n-\log_2 b} = b^{-1} N_n . \tag{13c}$$

From Eqs. (13a) and (13b) the relation

$$p_n \rightarrow p_{n-\log_2 b} = b p_n \tag{13d}$$

is obtained for the probability measure $p_n = l_n / L_n$. From Eqs. (13c) and (13d) it can be understood that N_n and $1/p_n$ are independent of H. In addition, the relations $\ln N_n \rightarrow \ln N_n - \ln b$ and $-\ln p_n \rightarrow -\ln p_n - \ln b$ are obtained from Eqs. (13c) and (13d), respectively. These relations imply that all points on log-log plots of N_n versus $1/p_n$ shift along the line whose slope is unity. That is the reason why the distribution curves for FBM traces are not *similar* but *congruent* to each other.

In the case of contraction maps, the subset is composed of crossing points among distribution curves and the line from the origin of coordinate axes. However, in this FBM case, the subset should be composed of crossing points among distribution curves and the line whose slope is unity because all subsets have the same scaling relations (13c) and (13d) due to the homogeneity of H_q. This composition of subsets inevitably leads to the result that all subsets have the same λ and h. Hence we obtain a point entropy spectrum for FBM traces. In order to obtain the values of λ and h, we show the n dependence of $\ln N_n$ and $-\ln p_n$ of the subset whose probability $P_n = N_n p_n$ is maximum [gray circles in Fig. 5(a)] in Fig. 6. The obtained λ and h are $\lambda = h = 0.691$. This value is very close to $\ln 2$. Of course this value becomes $\ln c$ if we define $n = \log_c M$, where c is a parameter.

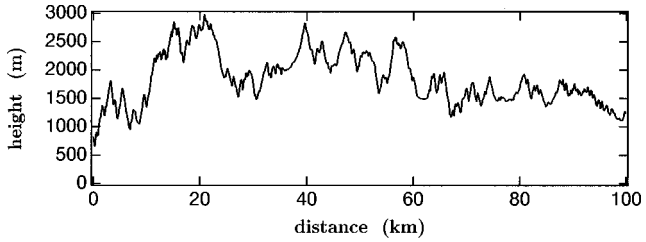

FIG. 7. Typical profile of the Hida mountains in Japan. The height variation is exaggerated.

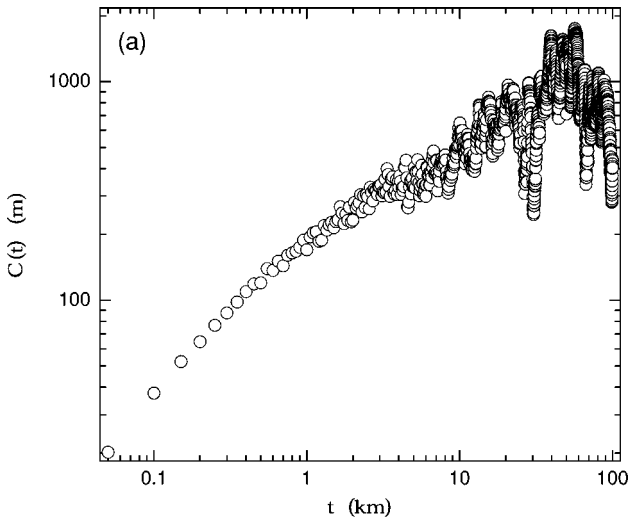

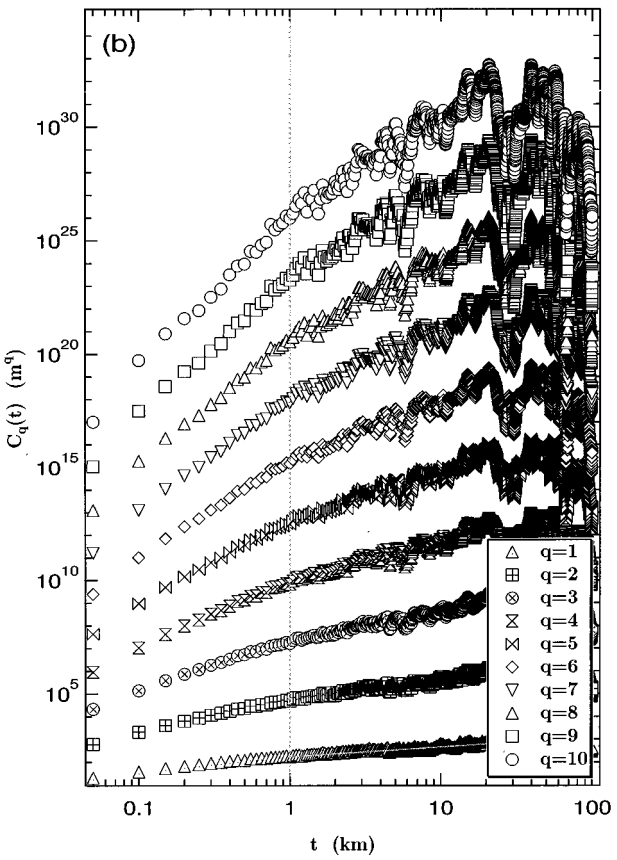

FIG. 8. (a) The height-height correlation function $C(t)$ obtained from the profile shown in Fig. 7. A crossover of the Hurst exponents is confirmed around the horizontal scale of 1 km. The Hurst exponents are obtained as $H_{1s}=0.669$ on a short length scale and $H_{1l}=0.428$ on a long length scale. (b) The qth-order height-height correlation function $C_q(t)$ obtained from the profile shown in Fig. 7.

B. Real mountain profiles

It has been reported that transect profiles of real mountain topography show self-affinity [5,6]. In particular, there is a

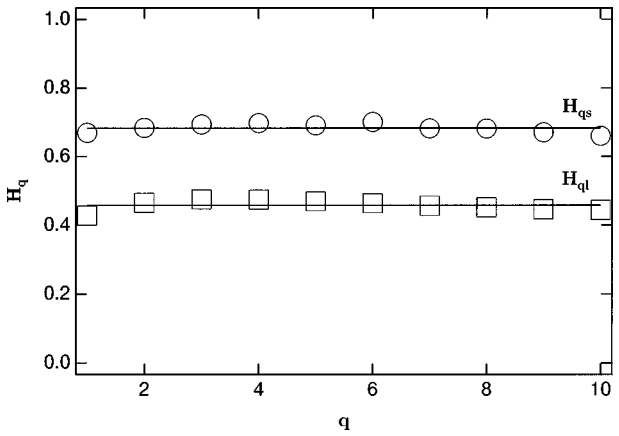

FIG. 9. H_q versus q obtained from the profile shown in Fig. 7. On both scales, H_q does not vary with q. The average generalized Hurst exponents are obtained as $H_{qs}=0.68\pm0.01$ and $H_{ql}=0.46\pm0.01$.

clear crossover of H in Mt. Shirouma in the Japanese Alps [5]. Matsushita and Ouchi have conjectured that this crossover is caused by the difference of roughening processes between short length scale and long length scale regimes. On short length scales, small-scale erosions due to, e.g., floods and earthquakes, produce the small-scale rough profile. On long length scales, large-scale folds due to the plate tectonics determine the large-scale rough structure. This crossover behavior indicates that the profile has two Hurst exponents. It is an interesting problem whether or not the entropy spectrum and H_q exhibit nontrivial characteristics.

We investigate the topography of the Hida mountains in the Japanese Alps. Figure 7 shows the typical profiles of the Hida mountains (very close to Mt. Shirouma) from the digital elevation map (50-m grid). The height-height correlation function $C(t)$ of this profile is shown in Fig. 8(a). A crossover of H is confirmed around the horizontal scale of 1 km. The value of 1 km is close to the crossover scale of Mt. Shirouma [5]. From Fig. 8(a) the Hurst exponent is obtained as H_{1s} (H_{qs} at $q=1$)$=0.669$ on a shorter length scale than 1 km and is obtained as H_{1l} (H_{ql} at $q=1$)$=0.428$ on a longer length scale than 1 km. In Sec. III A it is shown

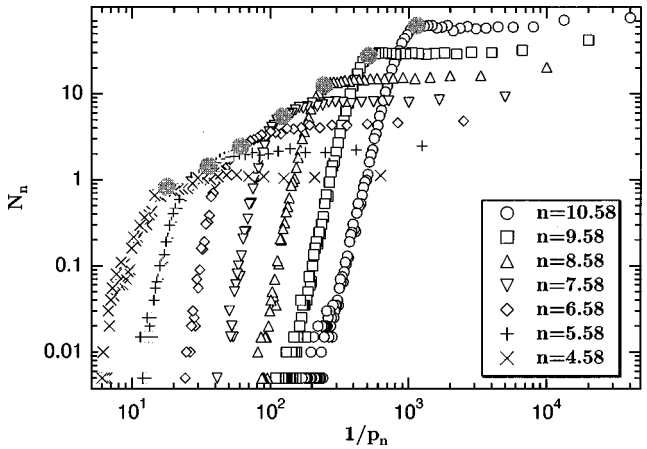

FIG. 10. Double logarithmic plots of N_n versus $1/p_n$ on the Hida mountains. Gray circles indicate the subset whose probability $P_n=N_np_n$ is the maximum.

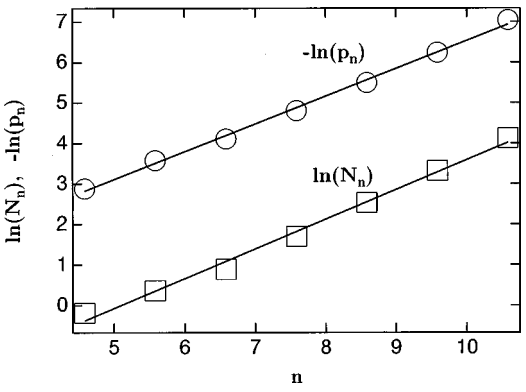

FIG. 11. n dependence of $\ln N_n$ and $-\ln p_n$ in the subset indicated by gray circles in Fig. 10. The slope of $\ln N_n$ and $-\ln p_n$ gives $h=0.732$ and $\lambda=0.685$, respectively.

that the q dependence of H_q is very important; therefore, we examine H_{qs} and H_{ql} from $C_q(t)$. $C_q(t)$ curves of various q values are shown in Fig. 8(b). We remove the data at large t ($t>20$ km) from the power-law fitting because of too much fluctuation. This fluctuation arises due to the finite-size effect. All $C_q(t)$ curves show the crossovers around $t\simeq1$ km. We show the q dependence of H_{qs} and H_{ql} in Fig. 9. It is shown that both H_{qs} and H_{ql} are constant ($H_{qs}=0.68\pm0.01$ and $H_{ql}=0.46\pm0.01$). This means that real mountain range topography has two unmixed Hurst exponents.

After the normalization of profiles to closed interval [0,1], we obtain log-log plots of N_n versus $1/p_n$ with the same definition of n (horizontal resolution level 2^{-n}), $N_n(p_n)$, and p_n (the probability measure being proportional to the height difference during normalized horizontal scale 2^{-n}) as in the FBM case (Fig. 10). Each distribution curve is an average of 200 profiles that are 50 m apart. Figure 10 is very similar to Fig. 5(a) and distribution curves seem to be congruent to each other. This affair implies that the scaling relations (13a)–(13d) are also satisfied in the Hida mountains. Therefore, the $C_q(t)$ curves of the Hida mountains should be fitted by the power law as mentioned in Fig. 8. Eventually, the above analysis method is easy and useful to discuss the condition of the scaling. From Figs. 9 and 10 the entropy spectrum of the Hida mountains becomes a point again. The horizontal distance of 1 km is equivalent to $n\simeq6.26$. No changes can be observed around $n\simeq6.26$ in Fig. 10. It should be recalled that these probability distribution curves are independent of H. We assume that the segments whose probability $P_n=N_np_n$ is maximum compose the subset (gray circles in Fig. 10). Figure 11 shows the n dependence of $\ln N_n$ and $-\ln p_n$ of this subset. The obtained values of h and λ are 0.732 and 0.685, respectively. Essentially these values should be the same value $\ln 2=0.691$; however, they deviate slightly.

IV. DISCUSSION

If we redefine Eqs. (7a)–(7c) as $l_n(\boldsymbol{x})=a^{n\delta(\boldsymbol{x})}$, $N_n(\boldsymbol{x})=a^{-nh(\boldsymbol{x})}$, and $p_n(\boldsymbol{x})=a^{n\lambda(\boldsymbol{x})}$, the $h(\lambda)$ spectrum becomes an analog of the multiaffine spectrum defined by Barabási *et al.* [15], i.e., entropy spectrum and multiaffine spectrum are essentially the same and our formulation of the entropy spectrum is the same as the thermodynamic one. $\delta(\boldsymbol{x})$, $h(\boldsymbol{x})$, and

$\lambda(\boldsymbol{x})$ correspond to γ, h (or f), and α, respectively, of the formalism of Barabási *et al.*

For self-similar fractals, the $h(\lambda)$ and $f(\alpha)$ spectra are different [19]. When the normalized length of the segment is assigned to the probability measure in the $f(\alpha)$ formalism, the singularity of each subset becomes unity and the $f(\alpha)$ spectrum becomes a point. There is only one length to characterize the segment in self-similar fractals, but there are two (vertical and horizontal) lengths in self-affine profiles. One can define the vertical length as the probability measure for each support (horizontal length) in self-affine profiles. Then the nontrivial $f(\alpha)$ spectrum can be obtained in self-affine profiles. According to this definition, the limit of $n\rightarrow\infty$ of our formulation and the limit of support size approaching zero of the multifractal formalism are the same; therefore, the $h(\lambda)$ and $f(\alpha)$ spectra become essentially the same in self-affine profiles. Our probability measure method (Figs. 4, 5, and 10) can classify profiles. If the mixing of Hurst exponents exists, the probability distribution curves become similar to each other like those of Fig. 4. If the mixing does not exist, they become congruent to each other like those of Figs. 5 and 10. We obtain the important relation $D_B=2-H_{q=1}$ for multiaffine profiles. This is a generalization of Eq. (3b).

We can consider another class of contraction maps that have no homogeneous horizontal intervals [23]. In that case the $h(\lambda)$ spectrum becomes different from the multiaffine spectrum. However, a specific application of that analysis method is difficult. This application is an open problem.

The Hida mountains has two unmixed Hurst exponents H_{qs} and H_{ql}. This seems to represent the transition from a mountain to a mountain range. The self-affine profile whose H satisfies $H<\frac{1}{2}$ ($H>\frac{1}{2}$) has persistence (antipersistence) in general [11,20]. $H_{qs}=0.68>\frac{1}{2}$ means that the profile has persistence on a short length scale. On this scale, the topography is certainly rough, but the up (or down) tendency continues because of the existence of a mountain. In contrast, H_{ql} satisfies $H_{ql}=0.46<\frac{1}{2}$, i.e., the topography has antipersistence on a long length scale. On this scale, ups and downs are repeated due to the jagged topography of many mountains in the mountain ranges. This consideration is consistent with the fact that there is no mountain that has a horizontal scale more than a few kilometers in the Hida mountains.

The relations (13a)–(13d) seem to be always satisfied in ordinary statistical self-affine profiles. We conjecture that almost all self-affine fractals in nature are statistically homogeneous ($H_q=$const). Namely, they have the point spectra in terms of the entropy spectrum. It seems that one Hurst exponent might correspond to one physical mechanism in natural self-affine objects. In the case of the Hida mountains, there are two Hurst exponents; however, two mechanisms (erosions and plate tectonics) affect different scales. Therefore, two Hurst exponents do not mix with each other. If the profile is produced by plural physical mechanisms affecting the same scale, the mixing of Hurst exponents will be observed and the entropy spectrum will become broad. The remaining interesting problem is whether or not there are such phenomena in nature. On the other hand, multiaffinity has been observed in a particular class of numerical simulation [24]. According to Ref. [24], multiaffinity arises from the kinetic surface roughening with power-law-distributed amplitudes of uncorrelated noise. This type of surface roughening has been proposed by Zhang [25]. He obtained the variable Hurst (or roughness) exponent by controlling the exponent of power-law-distributed amplitudes of uncorrelated noise. He conjectured that the experimentally observed larger Hurst exponent is a manifestation of this instability by power-law-distributed amplitudes of uncorrelated noise. We think that broad entropy spectra are obtained for such rough surfaces. Experimental and more detailed studies are future problems.

V. SUMMARY

Self-affine fractal profiles have been studied by the entropy spectrum method. First, generalized multiaffine profiles were investigated formally and broad entropy spectra were obtained from the profiles created by the generator that has plural contraction ratios in general. We find that the remaining subset at $n=\infty$ satisfies $D_B=2-H_{q=1}$.

FBM traces were analyzed with this method and the point entropy spectrum was obtained due to the homogeneity of H_q. In spite of the existence of fluctuating lengths of the segments, the entropy spectrum becomes a point, i.e., there are no fluctuations of either singularity or topological entropy. In addition, we show that real mountain profiles do not show multiaffinity in spite of the existence of the crossover of Hurst exponents. Therefore, the entropy spectrum of real mountain profiles also becomes a point spectrum.

ACKNOWLEDGMENTS

The authors wish to thank Professor S. Ohta, Professor M. Sano, and Professor M. Matsushita for useful discussions and comments.

[1] B. B. Mandelbrot, *The Fractal Geometry of Nature* (Freeman, San Francisco, 1982).
[2] B. B. Mandelbrot, D. E. Passoja, and A. J. Paullay, Nature (London) **308**, 721 (1984).
[3] H. Honjo and S. Ohta, Phys. Rev. E **49**, R1808 (1994).
[4] S. V. Buldyrev, A.-L. Barabasi, F. Caserta, S. Havlin, H. E. Stanley, and T. Vicsek, Phys. Rev. A **45**, R8313 (1992).
[5] M. Matsushita and S. Ouchi, Physica D **38**, 246 (1989).
[6] A. Czirók, E. Somfai, and T. Vicsek, Phys. Rev. Lett. **71**, 2154 (1993).
[7] *Dynamics of Fractal Surfaces*, edited by F. Family and T. Vicsek (World Scientific, Singapore, 1989).
[8] A.-L. Barabási and H. E. Stanley, *Fractal Concepts in Surface Growth* (Cambridge University Press, New York, 1995).
[9] B. B. Mandelbrot, Phys. Scr. **32**, 257 (1985).
[10] R. F. Voss, Physica D **38**, 362 (1989).
[11] J. Feder, *Fractals* (Plenum, New York, 1988).
[12] H. G. E. Hentschell and I. Procaccia, Physica D **8**, 435 (1983).
[13] T. C. Halsay, M. H. Jensen, L. P. Kadanoff, I. Procaccia, and B. I. Shraiman, Phys. Rev. A **33**, 1141 (1986).

[14] A.-L. Barabási and T. Vicsek, Phys. Rev. A **44**, 2730 (1991).
[15] A.-L. Barabási, P. Szépfalusy, and T. Vicsek, Physica A **178**, 17 (1991).
[16] M. Sano, S. Sato, and Y. Sawada, Prog. Theor. Phys. **76**, 945 (1986).
[17] J.-P. Eckmann and I. Procaccia, Phys. Rev. A **34**, 659 (1986).
[18] T. Bohr and D. Rand, Physica D **25**, 387 (1987).
[19] H. Honjo and M. Sano, Prog. Theor. Phys. **94**, 737 (1995).
[20] B. B. Mandelbrot and J. W. Van Ness, SIAM (Soc. Ind. Appl. Math.) Rev. **10**, 422 (1968).
[21] A. Castro e Silva and J. G. Moreira, Physica A **235**, 327 (1997).
[22] H.-O. Peitgen and D. Saupe, *The Science of Fractal Images* (Springer-Verlag, New York, 1988); J. C. Russ, *Fractal Surfaces* (Plenum, New York, 1994).
[23] H. Katsuragi and H. Honjo, Fractals **6**, 263 (1998).
[24] A.-L. Barabási, R. Bourbonnais, M. Jensen, J. Kertész, T. Vicsek, and Y.-C. Zhang, Phys. Rev. A **45**, R6951 (1992).
[25] Y.-C. Zhang, J. Phys. (Paris) **51**, 2129 (1990).